Dissipative variational quantum algorithms for Gibbs state preparation

Yigal Ilin^{1*} and Itai Arad²

¹Andrew and Erna Viterbi Department of Electrical and Computer Engineering,

Technion – Israel Institute of Technology, 3200003, Haifa, Israel and

²Centre for Quantum Technologies, National University of Singapore, 117543 Singapore, Singapore

In recent years, variational quantum algorithms (VQAs) have gained significant attention due to their adaptability and efficiency on near-term quantum hardware. They have shown potential in a variety of tasks, including linear algebra, search problems, Gibbs and ground state preparation. Nevertheless, the presence of noise in current day quantum hardware, severely limits their performance. In this work, we introduce dissipative variational quantum algorithms (D-VQAs) by incorporating dissipative operations, such as qubit RESET and stochastic gates, as an intrinsic part of a variational quantum circuit. We argue that such dissipative variational algorithms posses some natural resilience to dissipative noise. We demonstrate how such algorithms can prepare Gibbs states over a wide range of quantum many-body Hamiltonians and temperatures, while significantly reducing errors due to both coherent and non-coherent noise. An additional advantage of our approach is that no ancilla qubits are need. Our results highlight the potential of D-VQAs to enhance the robustness and accuracy of variational quantum computations on NISQ devices.

I. INTRODUCTION

In recent years, variational quantum algorithms (VQAs) have gathered significant research interest due to their adaptability and efficiency on near-term quantum hardware [1–10]. A typical VQA involves preparing a trial state on a quantum computer and calculating a cost function based on measurements taken from that state [1, 10–13]. As of today, VQAs are one of our best candidates for a useful early quantum advantage. Firstly, the framework is very rich and adaptive, and can be applied to many practically important problems. VQAs have been designed for various linear algebra problems [14–16], search problems [17], determining the ground state of a given Hamiltonian [18], singular value decomposition [19], fidelity estimation [20] and many other tasks [8, 11, 13, 21]. Secondly, the VQA framework leverages a significant portion of the computation to a classical side, allowing for much shallower quantum circuits that are crucial for our current day noisy devices [22, 23]. Finally, the variational nature of these algorithms provides some resilience against coherent errors, which are prevalent in today's quantum hardware [22, 24-27].

Despite the above strengths, VQAs have not yet demonstrated a convincing quantum advantage. Arguably, the main obstacle are the noise levels present in current day quantum hardware (although other challenges exist even in noiseless devices, see Ref. [28] and Refs. [29–31]). The accumulation of noise in a VQA circuit degrades its performance. Specifically, noncoherent noise, such as decoherence or amplitude damping, poses the greatest challenge, as coherent noise can largely be mitigated by the variational ansatz. In such cases, one must resort to error mitigation techniques (see

Refs. [32–37]) to rectify the effects of noise, which usually come at an exponential cost, thereby again limiting the performance of the VQA, or wait for error correction to become viable.

In this study, we expand the capabilities of variational quantum algorithms by incorporating dissipative operations in the variational circuits. We call the resulting framework dissipative VQA (D-VQA). Our main claim is that the introduction of these new elements can alleviate the effect of non-coherent noise, much like variational unitaries can fight coherent errors. A simple example of a dissipative operation within a quantum circuit is a midcircuit measurement, potentially followed by a qubit reset. The inclusion of such operations in quantum circuits has been investigated in various contexts, including local quantum channel learning [38], measurement-induced entanglement phase transitions [39], error mitigation through postselection [40], quantum steering for state preparation [41], non-equilibrium phase transitions [42], and others [43-45].

Here, we investigate the efficacy of dissipative VQA, where we introduce a variational dissipative operation, denoted as \mathcal{R}_i , alongside unitary gates. Our dissipative operation includes both a stochastic element (a probabilistic gate), together with a RESET operation. Specifically, it is a parametrized gate, denoted by $\mathcal{R}_i(p,\phi)$, which resets qubit i to the pure state $|\phi\rangle\langle\phi|$ with probability p. We demonstrate that incorporating such gates offers two significant advantages: 1) The inclusion of dissipative operations allows for the creation of mixed states, eliminating the need for ancilla qubits when the trial state of the VQA is mixed. 2) D-VQA circuits can mitigate some of the non-coherent errors, similar to how unitary VQAs mitigate coherent errors, resulting in better performance in the presence of noise. This resilience is particularly good when targeting states with low purity.

We demonstrate the advantages of our D-VQA ansatz through a simple toy model and a set of classical simu-

^{*} yigal.ilin@gmail.com

lations of variational Gibbs state preparation with high fidelity in both noisy and noiseless scenarios across a wide range of quantum many-body Hamiltonians.

The structure of this paper is as follows: In Sec. II, we provide a comprehensive background on Gibbs state preparation on quantum devices. In Sec. III, we introduce a single-qubit toy model of a quantum circuit used in a D-VQA scheme, demonstrating its noise resilience against non-coherent errors. We also present our global ansatz, which employs the $\mathcal R$ gate and general 2-local unitaries. Sec. IV outlines the numerical optimization scheme and defines the noise model used. Sec. V presents the numerical results. Finally, in Sec. VI we present our conclusions and discuss possible future research directions.

II. BACKGROUND

Throughout this work we consider the problem of preparing a Gibbs state on a quantum computer. Gibbs state preparation is a central problem in quantum computation and information of both theoretical and practical importance. Specifically, Gibbs states are used in quantum machine learning [46–50], quantum simulation [51, 52], and quantum optimization [53, 54], and for training quantum Boltzmann machines by sampling from a well-prepared Gibbs state [55–57].

Given a Hamiltonian H, its Gibbs state ρ_G at inverse temperature $\beta=1/k_BT$ is given by

$$\rho_G \stackrel{\text{def}}{=} \frac{1}{Z} e^{-\beta H},\tag{1}$$

where $Z \stackrel{\text{def}}{=} \text{Tr}(\exp(-\beta H))$ is the partition function.

There are various approaches for preparing a Gibbs state on a quantum computer, which can be broadly categorized into two types. The first type includes non-variational algorithms that steer the system toward the target Gibbs state. These algorithms may simulate the physical process of thermalization, as seen in Refs. [58–65], utilize imaginary time evolution like in Refs. [66, 67], or use Monte Carlo style Gibbs samplers as in Refs. [68, 69]. Other methods include thermal shadow tomography [70], sampling from the Gibbs state using cluster expansions [71], dissipative sampling [72], or various other approaches [73–77].

The second type consists of variational algorithms, where a classical optimization routine iteratively updates the parameters of the variational quantum circuit based on a cost function that measures the proximity of the system state to the desired Gibbs state [2, 4, 78, 79]. These algorithms may leverage approaches similar to non-variational algorithms, such as thermalization [26, 80], imaginary time evolution [26, 81], or Monte Carlo style methods [82], among others [3, 83]. Additionally, variational algorithms have been successfully combined with classical neural network architectures to enhance the clas-

sical component of Gibbs sampling algorithms, as shown in Refs. [84, 85].

Some variational algorithms are designed specifically for NISQ-type computers. These algorithms aim to prepare a Gibbs state using minimal quantum resources, such as the number of gates and measurements, often relying on heuristic approaches [84–93]. Most of these NISQ-type algorithms require ancillary qubits coupled to the system where the thermal equilibrium state is prepared.

The natural cost function for the variational algorithm is the Helmholtz free-energy function $\mathcal{F}(\rho) \stackrel{\text{def}}{=} \operatorname{Tr}(H\rho) - \beta^{-1}S(\rho)$, as it is minimized by the Gibbs state ρ_G [94]. While the energy term $\operatorname{Tr}(H\rho)$ is a local observable, which can be estimated efficiently on a quantum computer, the von-Neumman entropy term $S(\rho) \stackrel{\text{def}}{=} -\operatorname{Tr}(\rho \log \rho)$ is highly non-local, and cannot be estimated efficiently. Therefore, in variational algorithms for the Gibbs states one has to make additional assumptions and/or approximations when using the free energy cost function [86–93, 95–98], or resort to a different cost function altogether [99].

The main purpose of this work is to investigate which Gibbs states can be prepared with dissipative variational circuits and how the accuracy changes in the presence of noise. Specifically, we aim to study the *expressibility* of the proposed ansatz. We shall therefore ignore the question of efficiency in the cost function and use the *infidelity* of the resultant state with the ideal Gibbs state as a cost function. Nevertheless, our ansatz can readily accommodate other loss function choices, including those with gradients calculated on quantum hardware, such as in Refs. [89, 99].

III. DISSIPATIVE CIRCUITS AND NOISE RESILIENCE

In this section we describe the central building block of our circuit, which is the dissipative single-qubit \mathcal{R} gate. We study its noise resilience properties through a simple one qubit example, and then describe our global ansatz that uses the \mathcal{R} gate and general 2-local unitaries.

A. Dissipative gates and noise resilience

Our variational circuit is based on a specific dissipative gate, which is a single-qubit, probabilistic gate that combines a RESET gate and a general 1-qubit rotation. For brevity, we shall refer to it as the \mathcal{R} gate. When acting on qubit i, its action is described by the non-unital quantum channel

$$\mathcal{R}_i(p,\phi)[\rho] \stackrel{\text{def}}{=} (1-p)\rho + p|\phi\rangle\langle\phi| \cdot \text{Tr}_i(\rho).$$
 (2)

 $\mathcal{R}_i(p, \phi)$ resets qubit i to the state $|\phi\rangle\langle\phi|$ with probability $p \in [0, 1]$, and with probability 1 - p leaves the state

unchanged. Since $|\phi\rangle\langle\phi|$ is a pure state on the Bloch sphere, it is described by two angles. Together with p, it uses three parameters.

One advantage of variational dissipative quantum circuits over unitary circuits is their partial resilience to dissipative noise. To illustrate this, we consider a toy model system with one qubit, assuming a simple depolarizing noise model.

Let r be a vector in the Bloch ball, and $\sigma \stackrel{\text{def}}{=} (X, Y, Z)$ be the vector of Pauli matrices. Consider a situation in which the ideal circuit applies a single qubit unitary gate U to a mixed input state $\rho_0 = \frac{1}{2}(\mathbb{I} + |\mathbf{r}| \cdot Z)$, and takes it to the ideal output state ρ_1 :

$$\rho_1 = \mathcal{U}[\rho_0] = U \rho_0 U^{\dagger} = \frac{1}{2} (\mathbb{I} + \boldsymbol{r} \cdot \boldsymbol{\sigma}),$$

where \mathcal{U} is the channel corresponding to the unitary U, i.e., $\mathcal{U}[\rho] = U\rho U^{\dagger}$. For simplicity, we assume that a depolarizing noise channel, given by

$$\mathcal{N}[\rho] \stackrel{\text{def}}{=} (1 - \lambda)\rho + \lambda \operatorname{Tr}(\rho) \cdot \frac{\mathbb{I}}{2}, \tag{3}$$

acts on the qubit after each gate. In such case, we can look for a unitary V with a corresponding channel $\mathcal V$ such that $\mathcal N \circ \mathcal V(\rho_0)$ is as close as possible to the ideal state ρ_1 . For any one-qubit state $\tau = \frac{1}{2}(\mathbb I + \boldsymbol n \cdot \boldsymbol \sigma)$, the action of the depolarizing channel $\mathcal N$ is to shrink its Bloch radius, i.e., $\tau \to \mathcal N[\tau] = \frac{1}{2}\big(\mathbb I + (1-\lambda)\boldsymbol n \cdot \boldsymbol \sigma\big)$. Therefore, it is easy to see that the optimal unitary V will be V = U, and the optimal noisy output ρ_1' is

$$\rho_1' = \mathcal{N} \circ \mathcal{U}[\rho_0] = \mathcal{N}[\rho_1] = \frac{1}{2} (\mathbb{I} + (1 - \lambda) \mathbf{r} \cdot \boldsymbol{\sigma}).$$

In such case, the optimized noisy state suffers an error of

$$\|\rho_1 - \rho_1'\|_1 = \left\|\frac{1}{2}\lambda \boldsymbol{r} \cdot \boldsymbol{\sigma}\right\|_1 = \lambda \cdot |\boldsymbol{r}|.$$

Now assume that we can use the dissipative \mathcal{R} gate, and apply a circuit of the form $\mathcal{R} \circ \mathcal{U}$. Together with the noise, our circuit will apply the channel $\mathcal{N} \circ \mathcal{R} \circ \mathcal{N} \circ \mathcal{U}$ so that

$$ilde{
ho}_1 = \mathcal{N} \circ \mathcal{R} \circ \mathcal{N} \circ \mathcal{U}(
ho_0) = \mathcal{N} \circ \mathcal{R} ig[rac{1}{2} ig(\mathbb{I} + (1-\lambda) m{r} \cdot m{\sigma} ig) ig].$$

To optimize the circuit, we first fix the ϕ parameter of the \mathcal{R} gate to be such that $|\phi\rangle\langle\phi|=\frac{1}{2}(\mathbb{I}+\hat{r}\cdot\sigma)$, where $\hat{r}\stackrel{\mathrm{def}}{=}r/|r|$, and leave p unfixed. A simple calculation shows that

$$\begin{split} &\mathcal{R}\big[\frac{1}{2}\big(\mathbb{I} + (1-\lambda)\boldsymbol{r}\cdot\boldsymbol{\sigma}\big)\big] \\ &= \frac{1}{2}\big[\mathbb{I} + \big((1-p)(1-\lambda) + p/|\boldsymbol{r}|\big)\boldsymbol{r}\cdot\boldsymbol{\sigma}\big], \end{split}$$

and therefore,

$$\tilde{\rho}_1 = \frac{1}{2} \left[\mathbb{I} + (1 - \lambda) \left((1 - p)(1 - \lambda) + p/|\mathbf{r}| \right) \mathbf{r} \cdot \boldsymbol{\sigma} \right].$$

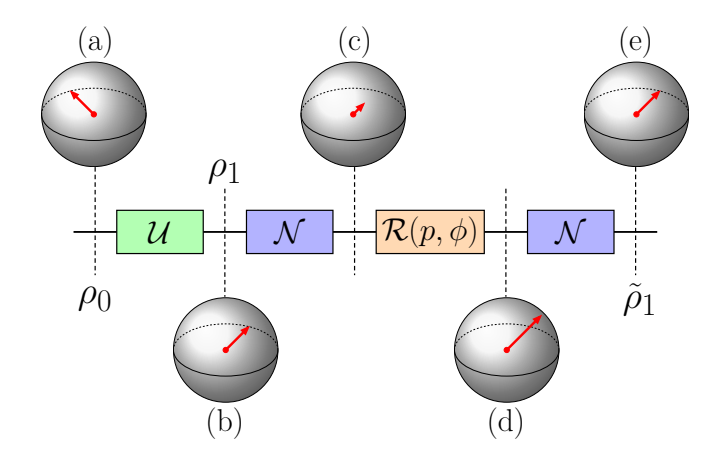


FIG. 1. Toy model illustrating a noisy single qubit circuit with the input state $\rho_0 = \frac{1}{2}(\mathbb{I} + |\mathbf{r}| \cdot Z)$, and the output state $\tilde{\rho}_1 = \mathcal{N} \circ \mathcal{R} \circ \mathcal{N} \circ \mathcal{U}(\rho_0)$. The red arrows in the Bloch balls (a-e) represent the mixed state after each operation. From left to right: (a) The input state ρ_0 . (b) Unitary channel \mathcal{U} rotates the input state to the ideal output state ρ_1 . (c) The depolarizing noise channel \mathcal{N} "shrinks" the vector \mathbf{r} . (d) The dissipative \mathcal{R} gate "expands" the vector \mathbf{r} beyond what is required to mitigate only the noise channel in (c). (e) The action of the noise channel \mathcal{N} applied after the \mathcal{R} gate reverts the state back to the ideal output of (b), such that in the best case $\tilde{\rho}_1 = \rho_1$.

It follows that as long as we can choose $p \in [0, 1]$ such that

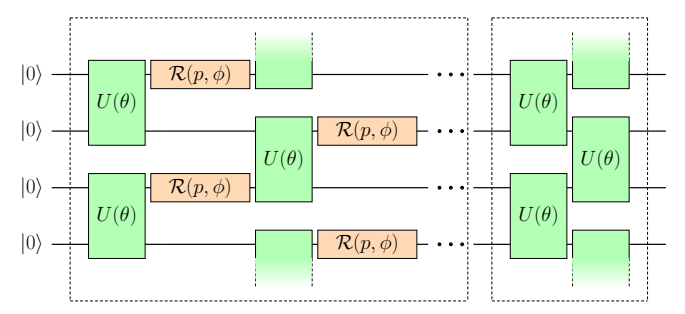
$$(1 - \lambda) ((1 - p)(1 - \lambda) + p/|r|) = 1,$$

we can fully cancel the effect of the dissipative noise. A straightforward calculation shows that this is possible iff $\lambda \leq 1 - |\mathbf{r}|$.

The above conclusion is further illustrated in Fig. 1, and can be understood intuitively as follows. The application of the noise increases the entropy of the state, or, equivalently, shrinks its Bloch radius |r|. Therefore, to counter it, we first inflate the Bloch radius using \mathcal{R} so that the subsequent decrease by \mathcal{N} will take us back to the ideal output. However, if the initial state is close to being pure (i.e., |r| is close to 1), we cannot increase its radius by much, and we cannot fully cancel the shrinkage due to \mathcal{N} . Therefore, for \mathcal{R} to cancel the noise, it must be that the distance of |r| from 1 is comparable to λ .

On a high level, the above analysis shows that the dissipative variational circuit behaves like the probabilistic error mitigation (PEC) [32, 100, 101], as it effectively inverts the noise channel. Unlike, PEC, however, it does this automatically without a prior characterization of the noise model. On the other hand, it can only apply inverse noise channels that are physical, and as such, it cannot fully correct high noise levels.

We conclude by noting that another potential advantage of using the dissipative \mathcal{R} gate in variational quantum circuits is that it can be seen as a stochastic, parameterized version of a mid-circuit measurement. As shown



Dissipative part, contains D repetitions Coherent part

FIG. 2. Dissipative circuit model for system size n=4 qubits arranged on a ring. The input state is initialized to $|0\rangle\langle 0|^{\otimes n}$. The dissipative parametrized layer is repeated D times, and followed by a single unitary (coherent) layer. The unitary gates $U(\theta)$ are general two-qubit gates. The parametrized probabilistic RESET gates are represented as non-unital channels $\mathcal R$ given in Eq. (2). The parameters θ, p, ϕ are different from gate to gate.

in Ref. [39], adding dissipation through random measurements can significantly increase the variance of gradients with respect to the circuit's parameters. This may help the classical optimization routine in VQA algorithms to avoid local minima and prevent rapidly decaying gradients, which may lead to barren plateaus [79, 102].

B. The dissipative circuit ansatz

Having defined the dissipative \mathcal{R} gate, our dissipative circuit anstaz follows a simple brick-wall architecture that is common in VQA circuits.

Alongside the dissipative \mathcal{R} gates, we use general twoqubit gates U, parameterized by a vector of rotation angles $\boldsymbol{\theta}$, applied on neighboring qubits. For a general unitary $U \in SU(4)$, there exists a standard KAK decomposition into three CX gates and 15 elementary single qubit rotations between them [103]. We used this decomposition and let each two-qubit unitary to have its own set of 15 rotation angles.

Using the dissipative \mathcal{R} gates and general SU(4) gates, our ansatz uses a brick-wall structure, described in Fig. 2. While we focus on the periodic 1D case, our results can be readily generalized to other types of lattices. From a high-level perspective, the circuit consists of two parts. The first part is the dissipative part, which consists of D even-odd brick-wall layers, where each layer is made of entangling SU(4) gates and dissipative gates (see Fig. 2). The second part is purely coherent, consisting of a single even-odd brick-wall layer of SU(4) gates. For a system size n, with D dissipative layers, our numerical experiments were performed on variational circuits with (18D+15)n parameters.

The division of the circuit into two parts, loosely follows the approach taken in Refs. [86, 87, 91, 92]. There, the first part prepares a mixed state of orthogonal states

(usually in the computational basis) with Boltzmann weights that approximate the weights of the target Gibbs state. This mixed state is then rotated to the actual Gibbs state using several layers of unitary gates. Similarly, the dissipative part of our circuit can be viewed as preparing a mixed state with the target Boltzmann weights, which is then rotated to the target Gibbs state by the coherent part. We note, however, that in our approach the dissipative part also contains many unitary rotations, which help align the eigenbasis of the initial mixed state with the target Gibbs state. This allows the coherent part to be relatively shallow at the expense of increasing the depth of the dissipative part, which, in view of Sec. III A, is important for achieving dissipative noise resilience.

We conclude this section by noting that our anstaz can be used on current day quantum computers. Indeed, our circuit is equivalent to an ensemble of circuit instances, each instance representing a different branch of the various $\mathcal{R}_i(p,\phi)$ probabilistic gates — either the identity operator or the reset operator $|\phi\rangle\langle\phi|\cdot \mathrm{Tr}_i(\rho)$. The latter can be implemented by a standard RESET to $|0\rangle\langle0|$ gate, followed by a local rotation $|0\rangle\to|\phi\rangle$. Therefore, to run the circuit, we first sample a sufficient number of instances, and then execute each of these instances on a quantum computer. The final output state generated by the ansatz is obtained by averaging the outputs of the sampled circuit instances.

IV. NUMERICAL SIMULATIONS

To evaluate the effectiveness of our dissipative variational circuit in preparing Gibbs states, we conducted several numerical simulations of it, together with simulations of other coherent anstazes. These simulations were performed both under ideal, noiseless conditions and using a simple noise model typically assumed for gate-based quantum computers like those offered by IBMQ [104]. In this section we describe the systems we simulated and their noise model, together with technical details on the optimization algorithm, and finally the numerical results.

A. Simulated systems

We simulated system sizes between n=2 to n=6 qubits arranged on a ring, with the initial state $\rho_0=|0\rangle\langle 0|^{\otimes n}$. In all our simulations, we considered the Gibbs states of 2-local translation invariant Hamiltonians defined on a ring of n qubits as:

$$H = \sum_{i=1}^{n} h_{i,i+1},\tag{4}$$

where $h_{i,i+1}$ is the same operator, with $||h_{i,i+1}|| \le 1$, acting on qubits i, i+1, with the n+1 qubit identified as

qubit 1. We note that while our target Gibbs Hamiltonians were translationally invariant, we did not impose translation invariance on the underlying parameters of the circuit, and let the optimizer pick the optimal parameters independently.

B. Noise model

For the noisy simulations of our ansatz, we assumed a local Markovian noise model without crosstalks. Since we have two distinct types of gates, there are two types of noises to consider: the noise in the two-qubit unitary gates U (using the KAK formula, which is a combination of CX and rotation gates [103]) and the noise in the non-unital single-qubit channel \mathcal{R} .

For the two-qubit unitary gates, we used a simplified noise model similar to those in quantum noise simulators like IBM's Qiskit [104, 105]. In this model, each qubit j has its own noise channel \mathcal{N}_j , so the global noise channel on n qubits factors into a tensor product of single-qubit noise channels $\bigotimes_{j=1}^n \mathcal{N}^{(j)}$. Each $\mathcal{N}^{(j)}$ combines two noise sources: dephasing (phase damping) and amplitude damping [106]. The dephasing noise model with parameter λ_j acting on a qubit j is defined as a Pauli noise channel:

$$\mathcal{N}_{dep}^{(j)}[\rho] \stackrel{\text{def}}{=} (1 - \lambda_j)\rho + \lambda_j Z \rho Z. \tag{5}$$

The amplitude damping noise model with parameter ω_j acting on qubit j is defined by:

$$\mathcal{N}_{amp}^{(j)}[\rho] \stackrel{\text{def}}{=} K_0(\omega_j)\rho K_0^{\dagger}(\omega_j) + K_1(\omega_j)\rho_j K_1^{\dagger}(\omega_j), \quad (6)$$

where

$$K_0(\omega_j) = \begin{pmatrix} 1 & 0 \\ 0 & \sqrt{1 - \omega_j} \end{pmatrix} \quad K_1(\omega_j) = \begin{pmatrix} 0 & \sqrt{\omega_j} \\ 0 & 0 \end{pmatrix}. \tag{7}$$

The dephasing parameters $\{\lambda_j\}_{j=1}^n$ and amplitude damping parameters $\{\omega_j\}_{j=1}^n$ were chosen to correspond to a low noise regime with values $\sim 10^{-3}$ and were randomly generated before each optimization run: each λ_j and ω_j were picked uniformly at random inside the range $[1,2]\times 10^{-3}$.

Given that the CX gates, which have the longest duration and highest error rates, dominate the noise in two-qubit unitaries [107, 108], we assumed that most noise originates from these gates. Consequently, each application of a CX gate in the general two-qubit unitaries U on qubits j and j+1 was followed by the noise channel $\mathcal{N}_j \otimes \mathcal{N}_{j+1}$, and each 1-qubit rotation was assumed ideal.

As the non-unital channel \mathcal{R} from Eq. (2) is accomplished by a regular RESET gate

$$\mathcal{R}_{i}(p, \boldsymbol{\phi})[\rho] = (1 - p)\rho + pU(\boldsymbol{\phi})|0\rangle\langle 0|U^{\dagger}(\boldsymbol{\phi}) \cdot \operatorname{Tr}_{i}(\rho),$$

where $U(\phi)$ is a single-qubit rotation taking $|0\rangle \rightarrow |\phi\rangle$, we modeled its noise by a noise model of the standard

RESET gate. Following Ref. [109], we assumed a phenomenological noise model where the reinitialization of the qubit to the $|0\rangle\langle 0|$ state might fail. Specifically, we upperbounded the activation probability p by a global value $p^*=0.99$, i.e., $p\leq p^*<1$, so that a prefect RESET is never possible.

C. Simulation method

Our simulations were done by evolving the full density matrix according to the dissipative variational circuit from Fig. 2, starting from the initial state $\rho_0 = |0\rangle\langle 0|^{\otimes n}$. This produced an output variational state $\rho(\theta, \mathbf{p})$, where θ represents the unitary rotation angles for both the \mathcal{R} gates and the two-qubit unitary gates, and \mathbf{p} are the activation probabilities of the \mathcal{R} gates. We then optimized the variational parameters to minimize the infidelity cost function

$$\Phi(\boldsymbol{\theta}, \boldsymbol{p}) \stackrel{\text{def}}{=} 1 - F(\rho(\boldsymbol{\theta}, \boldsymbol{p}), \rho_G), \tag{8}$$

where

$$F(\rho(\boldsymbol{\theta}, \boldsymbol{p}), \rho_G) \stackrel{\text{def}}{=} \left[\text{Tr} \sqrt{\sqrt{\rho(\boldsymbol{\theta}, \boldsymbol{p})} \rho_G \sqrt{\rho(\boldsymbol{\theta}, \boldsymbol{p})}} \right]^2$$
 (9)

is the fidelity between the variational state $\rho(\boldsymbol{\theta}, \boldsymbol{p})$ and the target Gibbs state ρ_G [110].

As said by the end of Sec. II, the main focus of this work is to check the *expressibility* of our dissipative circuit and its resilience to noise. Consequently, we allowed ourselves to choose the infidelity as the loss function, even though it is hard to estimate it efficiently on a quantum computer. Similarly, other measures of distinguishability, such as trace distance or relative entropy between the target and variational Gibbs states, can be equally employed to define the loss function [106].

After each simulation, gradients with respect to the variational parameters were computed using PyTorch's automatic differentiation engine [111]. The parameters were then updated using the Adam [112] stochastic optimization algorithm based on the infidelity cost function $\Phi(\theta, p)$.

The initial values of the variational parameters $\boldsymbol{\theta}$ were randomly drawn at uniform in range $[-\pi, \pi]$, and the initial activation probabilities \boldsymbol{p} were drawn at uniform in range [0, 1].

Heuristically, we fixed the maximum number of optimization steps to be 2000. We added another heuristic termination criterion for the optimization process, wherein the optimization ceased if at step i, the value of the loss function $\Phi < 10^{-3}$.

V. RESULTS

In this section we present the results of our numerical simulations for Gibbs state preparation using our dissipative ansatz for the ideal and noisy cases.

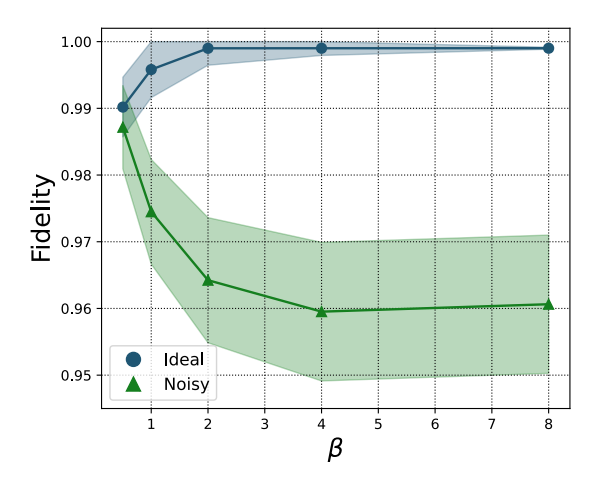


FIG. 3. The median fidelity between the estimated and target Gibbs states for 2-local translation-invariant Hamiltonians is shown for both noiseless (blue) and noisy (green) cases. Each data point represents the median fidelity of 200 random Hamiltonians. For each generated Hamiltonian, five optimization runs were performed with the best result taken for each case. The shaded area indicates the uncertainty, represented as one standard deviation.

A. Representation capabilities of the ansatz

We first investigated the expressibility of our ansatz, by checking how well it prepares the Gibbs state of a generic 2-local translation-invariant Hamiltonian, as defined by Eq. (4), across a broad range of inverse temperatures β . To this end, we fixed the system size to n=4 qubits and set the number of repetitions of the dissipative parametrized layer to D=n (see Fig. 2).

To evaluate the expressibility of our ansatz, we sampled N=1000 2-local translation-invariant Hamiltonians defined by Eq. (4) across five inverse temperatures: $\beta=0.5,1,2,4,8$. This range allowed us to examine both high and low temperature regimes. For each β value, 200 2-local translation-invariant Hamiltonians were sampled.

For each sample, we ran the optimization procedure, described in Sec. IV C, to minimize the cost function $\Phi(\theta, \mathbf{p})$ five times for the noiseless case and five times for the noisy case, using the noise model described in Sec. IV B. Each run was initialized with different variational parameters $\{\theta, \mathbf{p}\}$. We then selected the best result among these five runs for both the noisy and noiseless cases, respectively.

In Fig. 3 we present the median fidelity between the state estimated by our ansatz and the target Gibbs state as a function of the inverse temperature β . For each β value the median was calculated over 200 sampled Hamiltonians.

For the noiseless case, the most notable drop in the accuracy occurs at near room temperature corresponding to $\beta \sim 1$. As we discuss in the Sec. VB, when considering specific Hamiltonians, such dip appears also in other ansatzes [93, 113, 114] and may represent a fundamen-

tal limit on the representation power of the variational ansatzes. Nevertheless, for the ideal case, the median fidelity in Fig. 3 remains above 99% with uncertainty of at most $\sim 0.5\%$.

For the noisy case, the median fidelity gradually decreases towards 96% as β increases. Such behavior is expected, as for higher β values representing lower temperatures, the Gibbs state becomes more and more pure, and in light of Sec. III A, our dissipative circuit becomes less resilient to noise.

B. Ising and XY models

In this part we focused on two specific, well-studied models: the transverse field Ising (TFI) and the XY models. As in previous sections, we considered Gibbs states of translation invariant Hamiltonians arranged on a ring of n qubits.

The Hamiltonian of the transverse field Ising is given by:

$$H_{TFI} = -\sum_{j=1}^{n} X_j X_{j+1} - h \sum_{j=1}^{n} Z_j,$$
 (10)

where h represents the strength of the external field. In all our simulations we consider three values of h = 0.5, 1, 1.5. The Hamiltonian of the XY model is:

$$H_{XY} = -\sum_{j=1}^{n} \left[\frac{1+\gamma}{2} X_j X_{j+1} + \frac{1-\gamma}{2} Y_j Y_{j+1} \right] - h \sum_{j=1}^{n} Z_j,$$
(11)

where γ represents the degree of anisotropy with respect to the xy-plane [115]. In our simulations, in this section, we fixed h=0.5 and considered $\gamma=0.1,0.5,0.9$.

In all numerical trials that follow, for each data point, the optimization procedure was ran ten times with different initial parameter values, and the best result was selected.

1. Ising and XY models: system size dependence

In Fig. 4, we fixed the number of repetitions of the dissipative parametrized layer to D=n (see Fig. 2), and show how the precision of our ansatz varies for system sizes n=2,4,6, for the target Gibbs states of TFI and XY Hamiltonians for several inverse temperature values and for ideal and noisy cases.

In the noiseless case, Fig. 4 shows that our ansatz is capable of preparing the Gibbs state of the target Hamiltonian with fidelity > 99% for all values of β considered, for up to six qubits. Our noiseless ansatz results closely resemble the numerical results in Refs. [113, 114] for the TFI and XY Hamiltonians, respectively. The most notable drop in the fidelity for different system sizes occurs

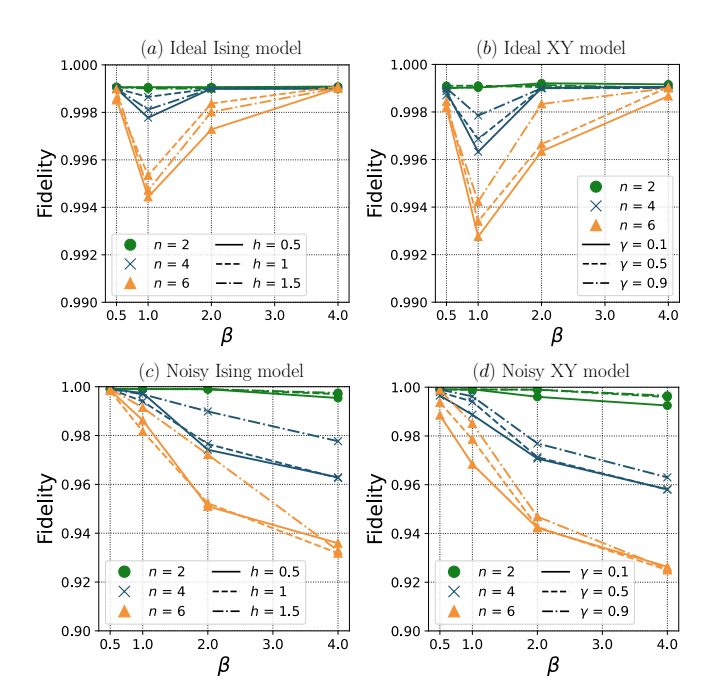


FIG. 4. Fidelity between the exact Gibbs state and the state produced by our ansatz, versus the inverse temperature β , for several system sizes n=2,4,6 and fixed dissipative layer depth D=n, for each system size. (a, c) Transverse field Ising model for ideal and noisy cases, respectively. (b, d) XY model for ideal and noise cases, respectively. For each point, ten optimization runs were performed with the best result taken.

at intermediate temperatures where $\beta \sim 1$. Such dip in accuracy was also observed in Refs. [113, 114], where the authors hinted that this can represent the limit of the ansatz's representation power. This limitation arises from the higher number of eigenstates needed to accurately represent the desired Gibbs state at intermediate temperatures.

For the noisy simulations, the noise parameters were set as described in Sec. IV B. Fig. 4 illustrates that the fidelity between the estimated and target Gibbs states gradually decreases with increasing values of β , corresponding to lower temperatures, similar to the trend observed in Fig. 3. As system size increases, the accuracy of the noisy ansatz significantly drops, particularly at lower temperatures. This is expected in light of Sec. III A, which demonstrates that the noise resilience of our dissipative ansatz drops as the target state becomes more and more pure. As the system size increases, these errors naturally accumulate.

2. Ising and XY models: circuit depth

In Fig. 5, we fixed the system size at n=6 and examined how the depth D of the dissipative parametrized layer affects the accuracy of our ansatz in the noiseless and noisy cases, for both the TFI Hamiltonian with h=1

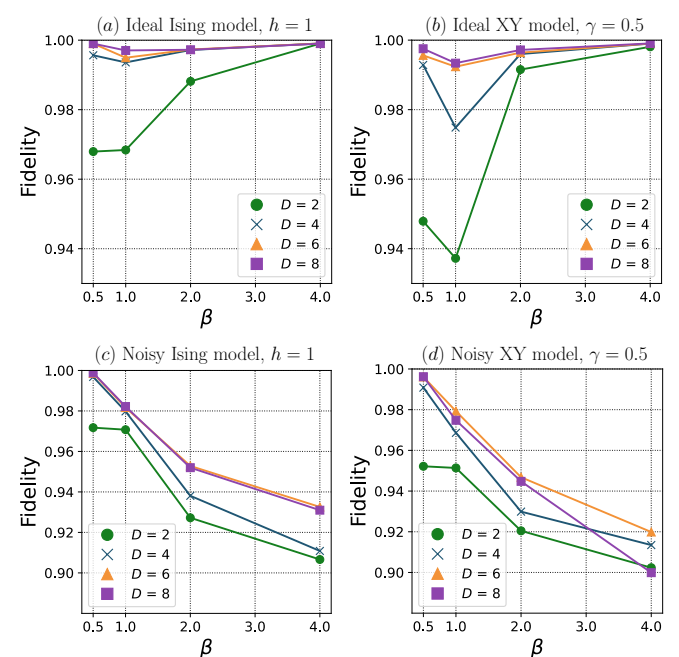


FIG. 5. Fidelity between the exact Gibbs state and the state produced by our ansatz, versus the inverse temperature β , for different depth values of the dissipative layer D=2,4,6,8 and for fixed system size n=6. (a,c) Transverse field Ising model for ideal and noisy cases with h=1, respectively. (b,d) XY model for ideal and noisy cases with $\gamma=0.5$, respectively. For each point, ten optimization runs were performed with the best result taken.

and the XY Hamiltonian with $\gamma = 0.5$.

For the noiseless case, shown in Fig. 5(a,b), the accuracy of our ansatz significantly increases as the depth D approaches the system size n. For the TFI Hamiltonian, a fidelity of over 99% is achieved at D=4, whereas for the XY Hamiltonian, this fidelity is reached only at D=6. This difference is due to the higher entanglement in the Gibbs state of the XY model, requiring deeper circuits to generate the necessary entanglement. For D=8, the fidelity only slightly increases for both models.

For the noisy case, shown in Fig. 5(c,d), the best accuracy is reached at D=n. However, unlike the noiseless case, where increasing the circuit depth from D=6 to D=8 resulted in a slight increase in accuracy, in the noisy case, increasing the depth from D=6 to D=8 may lead to a noticeable decrease in accuracy, as particularly evident from Fig. 5(d). This behavior is expected in the noisy case, as adding more layers may lead to an accumulation of errors that cannot be mitigated by the dissipative circuit, which might lead to an overall degradation in the fidelity.

3. Ising and XY models: comparison with unitary ansatzes

In Fig. 6, we compare the accuracy of our method with the full unitary ansatz proposed in Ref. [89]. The

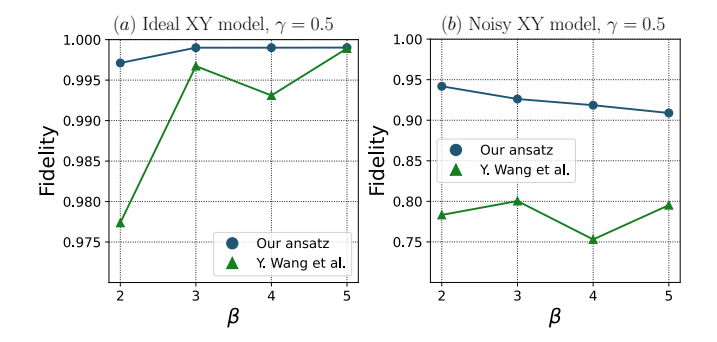


FIG. 6. Fidelity comparison between our ansatz and the ansatz presented in Fig. 7 in Ref. [89], versus the inverse temperature β , for the fixed system size n=6. (a) In the noiseless case, the ansatzes perform similarly at low temperatures. (b) Results for the noisy case, assuming low noise regime, the accuracy of our method gradually decreases for lower temperatures, while the ansatz presented in Fig. 7 in Ref. [89] reaches $\leq 80\%$ fidelity. For each point, ten optimization runs were performed with the best result taken.

comparison uses the XY model Hamiltonian defined in Eq. (11) on n=6 qubits with anisotropic parameter $\gamma=0.5$ and h=0.5.

For our circuits, we set D=6, and for the ansatz from Ref. [89], we also chose a depth parameter d=6, as shown in Fig. 7 of Ref. [89]. The ansatz from Ref. [89] uses a single ancilla qubit, requiring a total of 7 qubits for the Gibbs state preparation on n=6 qubits.

We tested both ansatzes under noiseless and noisy conditions, assuming a low noise level of $\sim 10^{-3}$ for the noisy case. Both ansatzes were tested at inverse temperatures $\beta=2,3,4,5$ because the ansatz from Ref. [89] underperformed at lower β values. This underperformance can be attributed to the fact that the specific ansatz from Fig. 7 in Ref. [89] was tested on a smaller system. Fig. 6 clearly demonstrates the advantage of using dissipative variational circuits over unitary circuits in the noisy case, due to their higher noise resilience.

Another comparison can be made between our results for the noisy transverse field Ising (TFI) model presented in Fig. 4(c) and the noisy simulation results presented in Ref. [91], for the case of the same TFI model. Although the noise model used for the TFI model simulations in Ref. [91] is not identical to the one we used, it is a simplified version derived from the IBMQ device backend. As demonstrated in Ref. [38], this noise model primarily consists of dephasing and amplitude damping processes. Therefore, although a direct comparison between the noisy TFI results in Ref. [91] and our noisy TFI model results in Fig. 4(c) is not possible, as it was in Fig. 6, we can still conclude that, generally, unitary VQAs do not perform well under noisy conditions.

VI. DISCUSSION AND OUTLOOK

In this article, we introduced the dissipative variational quantum algorithm (D-VQA) framework, which extends the capabilities of unitary variational quantum algorithms (VQAs) by incorporating a dissipative operation as an intrinsic component of the variational circuit. Specifically, we presented the dissipative \mathcal{R} gate, which re-initializes the single qubit state to a variational pure state with variational probability p. Through analytical analysis using a single-qubit toy model and various numerical examples, we demonstrated that incorporating such dissipative operations enhances the resilience of the variational circuit against both coherent and noncoherent errors. The resilience to coherent errors arises naturally from the unitary part of the variational circuit [22, 24–27], while the non-coherent noise resilience is directly attributed to the dissipative component.

Our numerical examples showed that a D-VQA-based ansatz can accurately prepare Gibbs states for a broad range of quantum many-body Hamiltonians across a wide spectrum of temperatures. We specifically focused on well-known quantum many-body models, such as the transverse field Ising model and the XY model. In the ideal noiseless case, our proposed D-VQA-based ansatz achieved at least the same degree of accuracy as the latest existing VQA-based ansatzes [89, 91–93]. In the noisy case, within the low-noise regime, our ansatz significantly outperformed the state-of-the-art unitary VQA-based ansatz from Ref. [89].

Although the low-noise regime is not yet available on publicly accessible quantum platforms, significant research efforts over the past years have achieved quantum gate fidelities exceeding 99.9%, suggesting that this noise regime will soon be attainable on NISQ devices [107, 116–118]. Moreover, our framework can be combined with either error mitigation or error correction techniques — and will require a lesser reduction in the noise levels to achieve a certain fidelity, in comparison with unitary VQAs.

Additionally, using D-VQA-based ansatzes, where the dissipative operation involves parametrized mid-circuit measurements, may help classical optimization routines to avoid barren plateaus [79, 102] by significantly increasing the variance of the gradients with respect to variational circuit parameters, as suggested by Ref. [39]. In this context, it would be interesting to investigate the extent to which D-VQA ansatzes exhibit resilience to the different types of barren plateaus, specifically the noise-induced barren plateaus identified in Ref. [119].

Our work leaves several open questions. It would be valuable to gain further theoretical understanding of D-VQAs by exploring more complex scenarios beyond the single-qubit toy model presented here. Specifically, understanding how entanglement between qubits influences the D-VQA circuit's resilience to non-coherent errors would be of great interest.

It would also be interesting to implement our D-VQA

ansatzes on real quantum hardware, potentially demonstrating high-fidelity Gibbs state preparation on a quantum device for systems larger than just a few qubits. Such demonstrations, coupled with further analytical investigations of D-VQAs, could provide more evidence for the importance of dissipative operations for noise resilience, and potentially influence future error mitigation and correction approaches.

Another direction of both theoretical and practical significance could be comparing our work with the probabilistic error correction (PEC) framework introduced in Refs. [32, 100, 101]. It would be interesting to explore how our D-VQA circuits can be integrated with the PEC framework to further enhance the noise resilience of the

resulting variational circuits. Although no mitigation method, including PEC, is perfectly scalable, integrating the PEC with the D-VQA framework might reduce the exponential cost associated with error mitigation.

ACKNOWLEDGEMENTS

We thank Amit Kam, Rotem Elimelech, Netanel Lindner and Yoav Sagi for enlightening discussions.

This research project was supported by the National Research Foundation, Singapore and A*STAR under its CQT Bridging Grant. It was also partially supported by the Helen Diller Quantum Center at the Technion – Israel Institute of Technology.

- A. Peruzzo, J. McClean, P. Shadbolt, M.-H. Yung, X.-Q. Zhou, P. J. Love, A. Aspuru-Guzik, and J. L. O'Brien, A variational eigenvalue solver on a photonic quantum processor, Nature Communications 5, 10.1038/ncomms5213 (2014).
- [2] E. Farhi, J. Goldstone, and S. Gutmann, A quantum approximate optimization algorithm (2014).
- [3] D. Wecker, M. B. Hastings, and M. Troyer, Progress towards practical quantum variational algorithms, Phys. Rev. A 92, 042303 (2015).
- [4] S. Endo, J. Sun, Y. Li, S. C. Benjamin, and X. Yuan, Variational quantum simulation of general processes, Phys. Rev. Lett. 125, 010501 (2020).
- [5] L. Bittel and M. Kliesch, Training variational quantum algorithms is np-hard, Phys. Rev. Lett. 127, 120502 (2021).
- [6] M. Benedetti, M. Fiorentini, and M. Lubasch, Hardware-efficient variational quantum algorithms for time evolution, Phys. Rev. Res. 3, 033083 (2021).
- [7] X. Bonet-Monroig, H. Wang, D. Vermetten, B. Senjean, C. Moussa, T. Bäck, V. Dunjko, and T. E. O'Brien, Performance comparison of optimization methods on variational quantum algorithms, Phys. Rev. A 107, 032407 (2023).
- [8] X. Yuan, S. Endo, Q. Zhao, Y. Li, and S. C. Benjamin, Theory of variational quantum simulation, Quantum 3, 191 (2019).
- [9] M. B. Hastings, D. Wecker, B. Bauer, and M. Troyer, Improving quantum algorithms for quantum chemistry (2014).
- [10] A. Kandala, A. Mezzacapo, K. Temme, M. Takita, M. Brink, J. M. Chow, and J. M. Gambetta, Hardwareefficient variational quantum eigensolver for small molecules and quantum magnets, Nature 549, 242–246 (2017).
- [11] Y. Li and S. C. Benjamin, Efficient variational quantum simulator incorporating active error minimization, Phys. Rev. X 7, 021050 (2017).
- [12] C. Hempel, C. Maier, J. Romero, J. McClean, T. Monz, H. Shen, P. Jurcevic, B. P. Lanyon, P. Love, R. Babbush, A. Aspuru-Guzik, R. Blatt, and C. F. Roos, Quantum chemistry calculations on a trapped-ion quantum simulator, Phys. Rev. X 8, 031022 (2018).

- [13] J. Romero, R. Babbush, J. R. McClean, C. Hempel, P. J. Love, and A. Aspuru-Guzik, Strategies for quantum computing molecular energies using the unitary coupled cluster ansatz, Quantum Science and Technology 4, 014008 (2018).
- [14] X. Xu, J. Sun, S. Endo, Y. Li, S. C. Benjamin, and X. Yuan, Variational algorithms for linear algebra, Science Bulletin 66, 2181–2188 (2021).
- [15] C. Bravo-Prieto, R. LaRose, M. Cerezo, Y. Subasi, L. Cincio, and P. J. Coles, Variational quantum linear solver, Quantum 7, 1188 (2023).
- [16] H.-Y. Huang, K. Bharti, and P. Rebentrost, Near-term quantum algorithms for linear systems of equations (2019).
- [17] K. M. Nakanishi, K. Mitarai, and K. Fujii, Subspacesearch variational quantum eigensolver for excited states, Phys. Rev. Res. 1, 033062 (2019).
- [18] M. Cerezo, K. Sharma, A. Arrasmith, and P. J. Coles, Variational quantum state eigensolver, npj Quantum Information 8, 10.1038/s41534-022-00611-6 (2022).
- [19] X. Wang, Z. Song, and Y. Wang, Variational quantum singular value decomposition, Quantum 5, 483 (2021).
- [20] R. Chen, Z. Song, X. Zhao, and X. Wang, Variational quantum algorithms for trace distance and fidelity estimation, Quantum Science and Technology 7, 015019 (2021).
- [21] S. McArdle, T. Jones, S. Endo, Y. Li, S. C. Benjamin, and X. Yuan, Variational ansatz-based quantum simulation of imaginary time evolution, npj Quantum Information 5, 10.1038/s41534-019-0187-2 (2019).
- [22] J. R. McClean, J. Romero, R. Babbush, and A. Aspuru-Guzik, The theory of variational hybrid quantum-classical algorithms, New Journal of Physics 18, 023023 (2016).
- [23] H. R. Grimsley, S. E. Economou, E. Barnes, and N. J. Mayhall, An adaptive variational algorithm for exact molecular simulations on a quantum computer, Nature Communications 10, 10.1038/s41467-019-10988-2 (2019).
- [24] K. Khodjasteh and L. Viola, Dynamically errorcorrected gates for universal quantum computation, Phys. Rev. Lett. 102, 080501 (2009).
- [25] K. Sharma, S. Khatri, M. Cerezo, and P. J. Coles, Noise

- resilience of variational quantum compiling, New Journal of Physics **22**, 043006 (2020).
- [26] O. Shtanko and R. Movassagh, Preparing thermal states on noiseless and noisy programmable quantum processors (2021).
- [27] J. Berberich, D. Fink, and C. Holm, Robustness of quantum algorithms against coherent control errors, Phys. Rev. A 109, 012417 (2024).
- [28] S. Lee, J. Lee, H. Zhai, Y. Tong, A. M. Dalzell, A. Kumar, P. Helms, J. Gray, Z.-H. Cui, W. Liu, M. Kastoryano, R. Babbush, J. Preskill, D. R. Reichman, E. T. Campbell, E. F. Valeev, L. Lin, and G. K.-L. Chan, Evaluating the evidence for exponential quantum advantage in ground-state quantum chemistry, Nature Communications 14, 1952 (2023).
- [29] M. Larocca, S. Thanasilp, S. Wang, K. Sharma, J. Bia-monte, P. J. Coles, L. Cincio, J. R. McClean, Z. Holmes, and M. Cerezo, A review of barren plateaus in variational quantum computing (2024).
- [30] E. R. Anschuetz and B. T. Kiani, Quantum variational algorithms are swamped with traps, Nature Communications 13, 10.1038/s41467-022-35364-5 (2022).
- [31] A. V. Uvarov and J. D. Biamonte, On barren plateaus and cost function locality in variational quantum algorithms, Journal of Physics A: Mathematical and Theoretical 54, 245301 (2021).
- [32] E. van den Berg, Z. K. Minev, A. Kandala, and K. Temme, Probabilistic error cancellation with sparse pauli–lindblad models on noisy quantum processors, Nature Physics 19, 1116–1121 (2023).
- [33] A. Seif, Z.-P. Cian, S. Zhou, S. Chen, and L. Jiang, Shadow distillation: Quantum error mitigation with classical shadows for near-term quantum processors, PRX Quantum 4, 010303 (2023).
- [34] A. Strikis, D. Qin, Y. Chen, S. C. Benjamin, and Y. Li, Learning-based quantum error mitigation, PRX Quantum 2, 040330 (2021).
- [35] Z. Cai, Quantum error mitigation using symmetry expansion, Quantum 5, 548 (2021).
- [36] W. J. Huggins, S. McArdle, T. E. O'Brien, J. Lee, N. C. Rubin, S. Boixo, K. B. Whaley, R. Babbush, and J. R. McClean, Virtual distillation for quantum error mitigation, Phys. Rev. X 11, 041036 (2021).
- [37] G. S. Ravi, K. N. Smith, P. Gokhale, A. Mari, N. Earnest, A. Javadi-Abhari, and F. T. Chong, Vaqem: A variational approach to quantum error mitigation, in 2022 IEEE International Symposium on High-Performance Computer Architecture (HPCA) (IEEE, 2022).
- [38] Y. Ilin and I. Arad, Learning a quantum channel from its steady-state, New Journal of Physics 26, 073003 (2024).
- [39] R. Wiersema, C. Zhou, J. F. Carrasquilla, and Y. B. Kim, Measurement-induced entanglement phase transitions in variational quantum circuits, SciPost Phys. 14, 147 (2023).
- [40] L. Botelho, A. Glos, A. Kundu, J. A. Miszczak, O. Salehi, and Z. Zimborás, Error mitigation for variational quantum algorithms through mid-circuit measurements, Phys. Rev. A 105, 022441 (2022).
- [41] D. Volya and P. Mishra, State preparation on quantum computers via quantum steering, IEEE Transactions on Quantum Engineering 5, 1–14 (2024).
- [42] E. Chertkov, Z. Cheng, A. C. Potter, S. Gopalakrishnan, T. M. Gatterman, J. A. Gerber, K. Gilmore, D. Gresh,

- A. Hall, A. Hankin, M. Matheny, T. Mengle, D. Hayes, B. Neyenhuis, R. Stutz, and M. Foss-Feig, Characterizing a non-equilibrium phase transition on a quantum computer, Nature Physics 19, 1799–1804 (2023).
- [43] M. DeCross, E. Chertkov, M. Kohagen, and M. Foss-Feig, Qubit-reuse compilation with mid-circuit measurement and reset, Phys. Rev. X 13, 041057 (2023).
- [44] F. Hua, Y. Jin, Y. Chen, S. Vittal, K. Krsulich, L. S. Bishop, J. Lapeyre, A. Javadi-Abhari, and E. Z. Zhang, Exploiting qubit reuse through mid-circuit measurement and reset (2022).
- [45] S. Brandhofer, I. Polian, and K. Krsulich, Optimal qubit reuse for near-term quantum computers, in 2023 IEEE International Conference on Quantum Computing and Engineering (QCE) (IEEE, 2023).
- [46] J. Biamonte, P. Wittek, N. Pancotti, P. Rebentrost, N. Wiebe, and S. Lloyd, Quantum machine learning, Nature 549, 195–202 (2017).
- [47] Y. Y. Lifshitz, E. Bairey, E. Arbel, G. Aleksandrowicz, H. Landa, and I. Arad, Practical quantum state tomography for gibbs states (2021).
- [48] C. Zoufal, A. Lucchi, and S. Woerner, Variational quantum boltzmann machines, Quantum Machine Intelligence 3, 10.1007/s42484-020-00033-7 (2021).
- [49] C. Zoufal, Generative quantum machine learning (2021).
- [50] G. Torlai and R. G. Melko, Machine-learning quantum states in the nisq era, Annual Review of Condensed Matter Physics 11, 325–344 (2020).
- [51] A. M. Childs, D. Maslov, Y. Nam, N. J. Ross, and Y. Su, Toward the first quantum simulation with quantum speedup, Proceedings of the National Academy of Sciences 115, 9456–9461 (2018).
- [52] E. Vernier, B. Bertini, G. Giudici, and L. Piroli, Integrable digital quantum simulation: Generalized gibbs ensembles and trotter transitions, Phys. Rev. Lett. 130, 260401 (2023).
- [53] R. D. Somma, S. Boixo, H. Barnum, and E. Knill, Quantum simulations of classical annealing processes, Phys. Rev. Lett. 101, 130504 (2008).
- [54] N. Mohseni, P. L. McMahon, and T. Byrnes, Ising machines as hardware solvers of combinatorial optimization problems, Nature Reviews Physics 4, 363–379 (2022).
- [55] N. Wiebe, A. Kapoor, and K. M. Svore, Quantum deep learning (2014).
- [56] M. Kieferová and N. Wiebe, Tomography and generative training with quantum boltzmann machines, Phys. Rev. A 96, 062327 (2017).
- [57] M. H. Amin, E. Andriyash, J. Rolfe, B. Kulchytskyy, and R. Melko, Quantum boltzmann machine, Phys. Rev. X 8, 021050 (2018).
- [58] D. Poulin and P. Wocjan, Sampling from the thermal quantum gibbs state and evaluating partition functions with a quantum computer, Phys. Rev. Lett. **103**, 220502 (2009).
- [59] E. Bilgin and S. Boixo, Preparing thermal states of quantum systems by dimension reduction, Phys. Rev. Lett. 105, 170405 (2010).
- [60] A. Riera, C. Gogolin, and J. Eisert, Thermalization in nature and on a quantum computer, Phys. Rev. Lett. 108, 080402 (2012).
- [61] H.-Y. Su and Y. Li, Quantum algorithm for the simulation of open-system dynamics and thermalization, Phys. Rev. A 101, 012328 (2020).

- [62] Z. Holmes, G. Muraleedharan, R. D. Somma, Y. Subasi, and B. Şahinoğlu, Quantum algorithms from fluctuation theorems: Thermal-state preparation, Quantum 6, 825 (2022).
- [63] K. Temme, T. J. Osborne, K. G. Vollbrecht, D. Poulin, and F. Verstraete, Quantum metropolis sampling, Nature 471, 87–90 (2011).
- [64] M.-H. Yung and A. Aspuru-Guzik, A quantum-quantum metropolis algorithm, Proceedings of the National Academy of Sciences 109, 754–759 (2012).
- [65] M. Metcalf, J. E. Moussa, W. A. de Jong, and M. Sarovar, Engineered thermalization and cooling of quantum many-body systems, Phys. Rev. Res. 2, 023214 (2020).
- [66] F. Verstraete, J. J. García-Ripoll, and J. I. Cirac, Matrix product density operators: Simulation of finite-temperature and dissipative systems, Phys. Rev. Lett. 93, 207204 (2004).
- [67] M. Motta, C. Sun, A. T. K. Tan, M. J. O'Rourke, E. Ye, A. J. Minnich, F. G. S. L. Brandão, and G. K.-L. Chan, Determining eigenstates and thermal states on a quantum computer using quantum imaginary time evolution, Nature Physics 16, 205-210 (2019).
- [68] C.-F. Chen, M. J. Kastoryano, F. G. S. L. Brandão, and A. Gilyén, Quantum thermal state preparation (2023).
- [69] D. Layden, G. Mazzola, R. V. Mishmash, M. Motta, P. Wocjan, J.-S. Kim, and S. Sheldon, Quantumenhanced markov chain monte carlo, Nature 619, 282–287 (2023).
- [70] L. Coopmans, Y. Kikuchi, and M. Benedetti, Predicting gibbs-state expectation values with pure thermal shadows, PRX Quantum 4, 010305 (2023).
- [71] N. M. Eassa, M. M. Moustafa, A. Banerjee, and J. Cohn, Gibbs state sampling via cluster expansions (2023).
- [72] D. Zhang, J. L. Bosse, and T. Cubitt, Dissipative quantum gibbs sampling (2023).
- [73] F. G. S. L. Brandão and M. J. Kastoryano, Finite correlation length implies efficient preparation of quantum thermal states, Communications in Mathematical Physics 365, 1–16 (2018).
- [74] A. N. Chowdhury and R. D. Somma, Quantum algorithms for gibbs sampling and hitting-time estimation (2016), arXiv:1603.02940 [quant-ph].
- [75] A. Gilyén, S. Lloyd, I. Marvian, Y. Quek, and M. M. Wilde, Quantum algorithm for petz recovery channels and pretty good measurements, Phys. Rev. Lett. 128, 220502 (2022).
- [76] S. Lu, M. C. Bañuls, and J. I. Cirac, Algorithms for quantum simulation at finite energies, PRX Quantum 2, 020321 (2021).
- [77] A. M. Alhambra, Quantum many-body systems in thermal equilibrium, PRX Quantum 4, 040201 (2023).
- [78] J. Tilly, H. Chen, S. Cao, D. Picozzi, K. Setia, Y. Li, E. Grant, L. Wossnig, I. Rungger, G. H. Booth, and J. Tennyson, The variational quantum eigensolver: A review of methods and best practices, Physics Reports 986, 1–128 (2022).
- [79] M. Cerezo, A. Arrasmith, R. Babbush, S. C. Benjamin, S. Endo, K. Fujii, J. R. McClean, K. Mitarai, X. Yuan, L. Cincio, and P. J. Coles, Variational quantum algorithms, Nature Reviews Physics 3, 625–644 (2021).
- [80] R. Sagastizabal, S. P. Premaratne, B. A. Klaver, M. A. Rol, V. Negîrneac, M. S. Moreira, X. Zou, S. Johri,

- N. Muthusubramanian, M. Beekman, C. Zachariadis, V. P. Ostroukh, N. Haider, A. Bruno, A. Y. Matsuura, and L. DiCarlo, Variational preparation of finite-temperature states on a quantum computer, npj Quantum Information 7, 10.1038/s41534-021-00468-1 (2021).
- [81] X. Wang, X. Feng, T. Hartung, K. Jansen, and P. Stornati, Critical behavior of the ising model by preparing the thermal state on a quantum computer, Physical Review A 108, 10.1103/physreva.108.022612 (2023).
- [82] T. L. Patti, O. Shehab, K. Najafi, and S. F. Yelin, Markov chain monte carlo enhanced variational quantum algorithms, Quantum Science and Technology 8, 015019 (2022).
- [83] J. Cohn, F. Yang, K. Najafi, B. Jones, and J. K. Freericks, Minimal effective gibbs ansatz: A simple protocol for extracting an accurate thermal representation for quantum simulation, Phys. Rev. A 102, 022622 (2020).
- [84] G. Verdon, M. Broughton, and J. Biamonte, A quantum algorithm to train neural networks using low-depth circuits (2017).
- [85] J.-G. Liu, L. Mao, P. Zhang, and L. Wang, Solving quantum statistical mechanics with variational autoregressive networks and quantum circuits, Machine Learning: Science and Technology 2, 025011 (2021).
- [86] J. Martyn and B. Swingle, Product spectrum ansatz and the simplicity of thermal states, Phys. Rev. A 100, 032107 (2019).
- [87] G. Verdon, J. Marks, S. Nanda, S. Leichenauer, and J. Hidary, Quantum hamiltonian-based models and the variational quantum thermalizer algorithm (2019).
- [88] D. Zhu, S. Johri, N. M. Linke, K. A. Landsman, C. Huerta Alderete, N. H. Nguyen, A. Y. Matsuura, T. H. Hsieh, and C. Monroe, Generation of thermofield double states and critical ground states with a quantum computer, Proceedings of the National Academy of Sciences 117, 25402–25406 (2020).
- [89] Y. Wang, G. Li, and X. Wang, Variational quantum gibbs state preparation with a truncated taylor series, Phys. Rev. Appl. 16, 054035 (2021).
- [90] J. Foldager, A. Pesah, and L. K. Hansen, Noise-assisted variational quantum thermalization, Scientific Reports 12, 10.1038/s41598-022-07296-z (2022).
- [91] M. Consiglio, J. Settino, A. Giordano, C. Mastroianni, F. Plastina, S. Lorenzo, S. Maniscalco, J. Goold, and T. J. G. Apollaro, Variational gibbs state preparation on nisq devices (2023).
- [92] M. Consiglio, Variational quantum algorithms for gibbs state preparation (2023).
- [93] J. Selisko, M. Amsler, T. Hammerschmidt, R. Drautz, and T. Eckl, Extending the variational quantum eigensolver to finite temperatures, Quantum Science and Technology 9, 015026 (2023).
- [94] F. Reif, Fundamentals of Statistical and Thermal Physics (McGraw-Hill, New York, 1965).
- [95] J. Wu and T. H. Hsieh, Variational thermal quantum simulation via thermofield double states, Phys. Rev. Lett. 123, 220502 (2019).
- [96] T. J. Sewell, C. D. White, and B. Swingle, Thermal multi-scale entanglement renormalization ansatz for variational gibbs state preparation (2022).
- [97] A. N. Chowdhury, G. H. Low, and N. Wiebe, A variational quantum algorithm for preparing quantum gibbs states (2020).
- [98] J. Y. Araz, R. G. Jha, F. Ringer, and B. Sambasivam,

- Thermal state preparation of the syk model using a variational quantum algorithm (2024).
- [99] A. Warren, L. Zhu, E. Barnes, and S. Economou, Adaptive variational algorithms for quantum gibbs state preparation, Bulletin of the American Physical Society 67 (2022).
- [100] K. Temme, S. Bravyi, and J. M. Gambetta, Error mitigation for short-depth quantum circuits, Phys. Rev. Lett. 119, 180509 (2017).
- [101] R. S. Gupta, E. v. d. Berg, M. Takita, D. Riste, K. Temme, and A. Kandala, Probabilistic error cancellation for dynamic quantum circuits (2023).
- [102] J. R. McClean, S. Boixo, V. N. Smelyanskiy, R. Babbush, and H. Neven, Barren plateaus in quantum neural network training landscapes, Nature Communications 9, 10.1038/s41467-018-07090-4 (2018).
- [103] F. Vatan and C. Williams, Optimal quantum circuits for general two-qubit gates, Phys. Rev. A 69, 032315 (2004).
- [104] Ibm quantum. https://quantum-computing.ibm.com/, 2022 (2022).
- [105] Qiskit: An open-source framework for quantum computing (2022).
- [106] M. A. Nielsen and I. L. Chuang, Quantum computation and quantum information (Cambridge university press, 2010).
- [107] M. Kjaergaard, M. E. Schwartz, J. Braumuller, P. Krantz, J. I.-J. Wang, S. Gustavsson, and W. D. Oliver, Superconducting qubits: Current state of play, Annual Review of Condensed Matter Physics 11, 369 (2020), https://doi.org/10.1146/annurev-conmatphys-031119-050605.
- [108] P. Jurcevic, A. Javadi-Abhari, L. S. Bishop, I. Lauer, D. F. Bogorin, M. Brink, L. Capelluto, O. Günlük, T. Itoko, and N. Kanazawa, Demonstration of quantum volume 64 on a superconducting quantum computing system, Quantum Science and Technology 6, 025020 (2021).
- [109] B. Rost, L. Del Re, N. Earnest, A. F. Kemper, B. Jones, and J. K. Freericks, Demonstrating robust simulation of driven-dissipative problems on near-term quantum computers, arXiv, arXiv:2108.01183 (2021).
- [110] A. Uhlmann, Transition probability (fidelity) and its relatives, Foundations of Physics 41, 288–298 (2010).

- [111] A. Paszke, S. Gross, F. Massa, A. Lerer, J. Bradbury, G. Chanan, T. Killeen, Z. Lin, N. Gimelshein, L. Antiga, A. Desmaison, A. Kopf, E. Yang, Z. DeVito, M. Raison, A. Tejani, S. Chilamkurthy, B. Steiner, L. Fang, J. Bai, and S. Chintala, Pytorch:an imperative style, high-performance deep learning library, in Advances in Neural Information Processing Systems 32 (Curran Associates, Inc., 2019) pp. 8024–8035.
- [112] D. P. Kingma and J. L. Ba, Adam: A method for stochastic optimization, 3rd International Conference on Learning Representations, ICLR 2015 - Conference Track Proceedings, 1 (2015), arXiv:1412.6980.
- [113] M. Consiglio, J. Settino, A. Giordano, C. Mastroianni, F. Plastina, S. Lorenzo, S. Maniscalco, J. Goold, and T. J. G. Apollaro, Variational Gibbs State Preparation on NISQ devices, arXiv (2023), arXiv:2303.11276.
- [114] M. Consiglio, Variational Quantum Algorithms for Gibbs State Preparation, arXiv (2023), arXiv:2305.17713.
- [115] E. Lieb, T. Schultz, and D. Mattis, Two soluble models of an antiferromagnetic chain, Annals of Physics 16, 407 (1961).
- [116] E. Zahedinejad, J. Ghosh, and B. C. Sanders, High-fidelity single-shot toffoli gate via quantum control, Phys. Rev. Lett. 114, 200502 (2015).
- [117] T. Xie, Z. Zhao, S. Xu, X. Kong, Z. Yang, M. Wang, Y. Wang, F. Shi, and J. Du, 99.92%-fidelity cnot gates in solids by noise filtering, Phys. Rev. Lett. 130, 030601 (2023).
- [118] E. J. Zhang, S. Srinivasan, N. Sundaresan, D. F. Bogorin, Y. Martin, J. B. Hertzberg, J. Timmerwilke, E. J. Pritchett, J.-B. Yau, C. Wang, W. Landers, E. P. Lewandowski, A. Narasgond, S. Rosenblatt, G. A. Keefe, I. Lauer, M. B. Rothwell, D. T. McClure, O. E. Dial, J. S. Orcutt, M. Brink, and J. M. Chow, High-fidelity superconducting quantum processors via laser-annealing of transmon qubits (2020).
- [119] S. Wang, E. Fontana, M. Cerezo, K. Sharma, A. Sone, L. Cincio, and P. J. Coles, Noise-induced barren plateaus in variational quantum algorithms, Nature Communications 12, 10.1038/s41467-021-27045-6 (2021).